Open Access Full Text Article

ORIGINAL RESEARCH

Spray with Nitric Oxide Donor Accelerates Wound Healing: Potential Off-the-Shelf Solution for Therapy?

Alexandra Igrunkova[1,2], Alexey Fayzullin[1,2], Semyon Churbanov[1], Polina Shevchenko[1], Natalia Serejnikova [1,2], Natalia Chepelova [1,2], Dmitry Pahomov[3], Ekaterina Blinova[4], Karen Mikaelyan[1], Victoria Zaborova[5,6], Konstantin Gurevich [7], Aleksandr Urakov [8,9], Anatoly Vanin[1], Peter Timashev[1,2,10], Anatoly Shekhter[1]

[1]Institute for Regenerative Medicine, Sechenov First Moscow State Medical University, Moscow, Russian Federation; [2]World-Class Research Center "Digital Biodesign and Personalized Healthcare", Sechenov First Moscow State Medical University, Moscow, Russian Federation; [3]Department of Operative Surgery and Topographic Anatomy, Sechenov First Moscow State Medical University, Moscow, Russian Federation; [4]Department of Faculty Surgery, Ogarev Mordovia State University, Saransk, Republic of Mordovia, Russian Federation; [5]Institute of Clinical Medicine, Sechenov First Moscow State Medical University, Moscow, Russian Federation; [6]Laboratory of Sports Adaptology, Moscow Institute of Physics and Technology, Dolgoprudny, Moscow Region, Russian Federation; [7]UNESCO Chair "Healthy life style for sustainable development", Moscow State University of Medicine and Dentistry, Moscow, Russian Federation; [8]Department of General and Clinical Pharmacology, Izhevsk State Medical Academy, Izhevsk City, Udmurt Republic, Russian Federation; [9]Department of Modeling and Synthesis of Technological Processes, Institute of Applied Mechanics, Udmurt Federal Research Center of the Ural Branch of the Russian Academy of Sciences, Izhevsk City, Udmurt Republic, Russian Federation; [10]Department of Chemistry, Lomonosov Moscow State University, Moscow, Russian Federation

Correspondence: Aleksandr Urakov, Department of General and Clinical Pharmacology, Izhevsk State Medical Academy, Kommunarov str., 281, Izhevsk City, Udmurt Republic, 426034, Russian Federation, Tel +011 79127600939, Email urakoval@live.ru

Background: Ditrosyl iron complexes (DNIC) are endogenous donors of nitric oxide. The possibility of their application to stimulate regeneration has been studied for more than 15 years. However, the most effective dose and form of delivery have not yet been determined.

Purpose: The aim of this research was to develop a spray form of DNIC that accelerates wound healing.

Methods: We prepared a series of DNIC sprays with spray dosages of 10, 50 and 100 µg. We modelled full-thickness skin wounds in 24 Wistar rats and treated them with distilled water (n = 6), 10 (n = 6), 50 (n = 6) and 100 µg (n = 6) for three post-operative days. On the fourth day, the excised wound tissues were studied by morphological, immunohistochemical and morphometric methods.

Results: We demonstrated that 50 µg of DNIC spray had the most beneficial effect on wound healing: the thickness of the granulation tissue layer was 140% higher, vimentin positive fibroblasts predominated and the intensity of inflammation was significantly lower than in the control. There was a dose-dependent decrease in the functional activity of mast cells in the experimental groups compared to the control.

Conclusion: DNIC spray is a potential effective dosage form for the treatment of large-area skin lesions.

Keywords: wound, infection, drug, resistance, research and development, nitric oxide, spray, healing

Introduction

Nitric oxide (NO) is a highly active gaseous signaling molecule that is synthesized by NO synthases and mediates many physiological processes, from vasodilation to signal transmission in neurons.[1,2] In addition, NO has a bactericidal effect, the ability to activate cellular and humoral immunity, induces the proliferation and synthetic activity of fibroblasts, activates the proliferation of keratinocytes and the antioxidant system.[3–7] The variety of these effects provides NO comprehensive effect in various stages of wound healing and accelerates regeneration.

Currently, there are three distinct ways for increasing the concentration of NO in wound tissues: the application of inductors of NO synthesis, NO-containing gas flows, and donor molecules.[7–11] Using NO donors is one of the most promising and actively developing areas because of the large variety of donor chemical compounds, investigated

349

Graphical Abstract
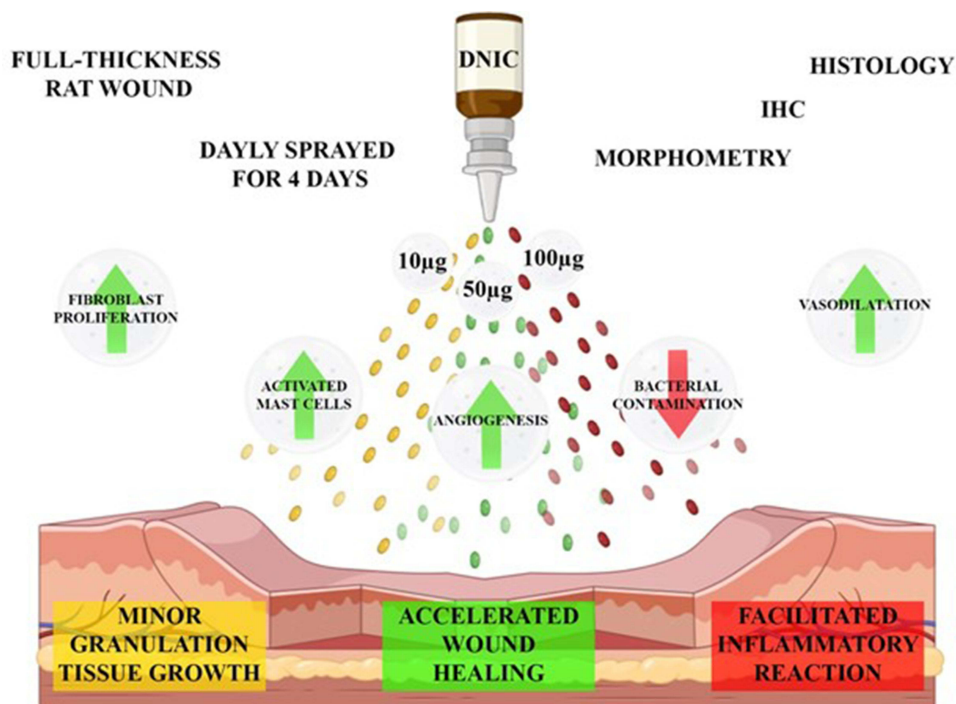
pharmaceutical modifications, and the possibility of inclusion in implantable constructs.[5,11–14] Endogenous molecules are of particular interest among other existing NO donors since they have their own signaling activity impacting tissue regeneration and metabolism even before the release of NO molecules.

Dinitrosyl iron complexes (DNIC) are the most abundant nitric oxide derivatives in living organisms among all endogenous donors. These stable complexes can act as free radical traps, regulate gene expression, apoptosis, and iron metabolism.[15,16] They can be easily synthesized chemically in mononuclear (M-DNIC) or binuclear forms (B-DNIC). The latter is formed as a result of the binding of two iron-dinitrosyl $[Fe_2(NO)_2]$ fragments of DNIC with bridging thiol sulfur atoms $[(RS)2Fe_2(NO)_4]$. The reaction results in pairing of the spins of iron atoms, making it impossible to detect B-DNIC by the electron paramagnetic resonance.[16,17]

Vanin et al showed that most DNICs with thiol-containing ligands formed in animal tissues are in binuclear form.[17] They are formed from relatively low concentrations of endogenously synthesized NO (about 50 nM) under physiological conditions. Integration of NO into DNIC protects it from unspecific oxidation, provides transport and interaction with specific targets. However, NO molecules in DNIC can be oxidized to the nitrosonium cation (NO+) remaining in the complex and taking part in the S-nitrosylation of thiols, other endogenous signaling molecules.[18] All in all, DNICs with thiol-containing ligands act as NO donors and nitrosonium cations in accordance with their resonance structures $[(RS-)2Fe_2+(NO+)(NO)]+$ (M-DNIC form) and $[(RS-)2Fe_2+2(NO+)2(NO)_2]4+$ (B-DNIC form).[16] In general, NO molecules have a beneficial regulatory effect on living tissues, while nitrosonium cations impact is cytotoxic and anti-regenerative.

DNIC signaling activity includes hypotensive and vasodilating effects,[19] prevention of platelet aggregation,[20] protection of myocardiocytes from hypoxic damage,[21,22] stimulation of long-term erection,[23] inhibition of endometrioid tumor growth,[24,25] induction of apoptosis in various tumor cell lines and facilitate the cytotoxic effect of radiation therapy.[26,27] So, the application of DNIC in a wide range of medical fields, from cardiology to oncology, has been studied for more than 15 years. Despite the proven efficacy, there is no evidence in the literature of the most effective dose of DNIC for healing skin wounds. Moreover, in most studies, DNIC was delivered systemically by intravenous

administration or by injections of the wound bottom, which is associated with systemic side-effects and prevents the translation of the results into clinical practice.[7,13,28]

Transdermal sprays and aerosols lack these limitations, making them attractive alternatives for DNIC delivery. They usually comprise a solution of active substance and volatile diluent. The volatile solvent carries the drug into the wound surface and, as it evaporates, an increase in the thermodynamic activity of the drug occurs, and the concentration increases.[29] Sprays have been used to treat skin conditions with antibacterial drugs,[30] hemoglobin[31] and even autological cells.[32] Despite the proven pro-regenerative effects and the potential to treat vast areas of the skin, the spray form of DNIC has not been developed or studied before. Also, unlike gels, patches, membranes, scaffold et al, the spray is the easiest developed delivery form and can be named a potential off-the-shelf solution for therapy.

This work aimed to develop a spray form of the nitric oxide donor to accelerate wound healing.

Materials and Methods
B-DNIC with Glutathione Synthesis
Gaseous NO was obtained by a reaction of ferrosulfate (Fluka, Buchs, Switzerland) with sodium nitrite (Sigma, St. Louis, USA) in 0.1 M HCl with subsequent purification of gaseous NO by low-temperature sublimation in an evacuated glass system. B-DNIC with glutathione was synthesized by a reaction of Fe^{2+} and glutathione (Sigma, St. Louis, USA) with gaseous NO at 150 mmHg pressure and molar Fe^{2+}: GSH ratio of 1:3 in a Thunberg apparatus as described in.[17] After dissolution of the ferrous sulfate solution (0.5 mL) in distilled water and loading of the glutathione solution (4.5 mL) in 15 mM HEPES pH 7.4 into the upper and bottom chambers of the Thunberg apparatus, the tube was evacuated and NO was injected. Both solutions in the apparatus were mixed in the presence of NO and shaken for 5 min after which NO was evacuated from the apparatus.

B-DNIC-Glutathione Characterization
B-DNIC concentrations were determined by the amount of iron (5 mM) used for B-DNIC synthesis. Additionally, the concentrations of synthesized B-DNIC were determined by the optical method from the intensity of specific absorption at 310 and 360 nm with extinction coefficients equal to 4600 and 3700 M-1 cm-1 (as calculated per one iron –dinitrosyl fragment in B-DNIC).[17] Optical measurements were carried out on a UV-2501PC spectrophotometer (Shimadzu Europa GmbH, Germany) using a flat quartz cuvette with an optical path of 10 mm. All the measurements were performed at ambient temperature.

Spray Solution Preparation and Characterization
Solutions were prepared by dissolving lyophilized DNIC-glutathione powder in sterile PBS at room temperature. The concentrations of the prepared solutions were 0.00001 g/L, 0.00005 g/L, 0.0001 g/L defining single spraying dosage of DNIC in a 3 cm^2 animal wound area as 10 μg, 50 μg, and 100 μg, respectively (or 3.33 μg, 16.6 μg, and 33.3 μg of the active substance were per 1 cm^2). The solutions were aliquoted into 4 plastic pump spray bottles of 50 mL (BX202005C, Ningbo Beixuan International Trading Co., Ltd) and stored at −70°C until applied. One spray sample of each DNIC concentration was used for in vitro analyses.

For sprayability evaluation, the solutions with different DNIC dosages were dyed with methylene blue. Then, the sprayer pump was fixed in a tripod at an angle of 45° and a distance of 10 cm to a paper. The 4th spray of every solution was directed to the paper, maximum (Dmax) and minimum (Dmin) diameters of its pattern were measured to calculate the ovality ratio (Ovality) by the following formula: Ovality = Dmax/Dmin. We repeated 5 times for all the spray concentrations.

Also, we assessed the stability of dosage in the single sprayed volume. The solution was sprayed onto a 5 cm diameter Petri dish at a 45° angle from a 10 cm distance. Then the dose was dried and weighed. Ten repetitions were performed. Using the Teflon ring with a fixed inner diameter 30mm and DNIC solutions stained with methylene blue, we determined the optional distance and angle for spraying the whole dose to the wound area. Degradation of the substance

in a solution with a DNIC mass fraction of 100 μg was assessed using a Multiskan FC Microplate Photometer (Thermo Scientific, USA) at a wavelength of 310 nm at 37°C.

Surgical Procedures

The in vivo experiment was approved by the Local Ethical Committee of the I.M. Sechenov First Moscow State Medical University. All animal studies were conducted in full conformity with the International Guiding Principles for Biomedical Research Involving Animals (Geneva, 1990).

We modeled full-thickness skin wounds in 24 male Wistar rats (180–220 g). A 25% urethane solution (Sigma, St. Louis, USA) was injected intraperitoneally for anesthesia, 80 mg of urethane per 100 g of animal weight. The anesthetized animals were fixed on a special operating table. A circle with a diameter of 8–10 mm was excised down to the fascia in the interscapular space. A Teflon ring with an inner diameter of 30 mm was implanted into the resulting defect, after which the outer diameter of the ring was covered with perforated plastic wrap to prevent drying, external contamination, and wound contraction. All the wounds had an area of 3 cm^2.

All animals were divided into four groups, with 6 rats in each. On days 1, 2, 3 after the operation, the animals were injected with a sedating solution of ZOLETIL 100 (VIRBAC, France), the protective film was removed from the surface of the ring. Then, distilled water (control) or a thawed at the room temperature solutions aliquots containing 10 μg, 50 μg, or 100 μg of DNIC were sprayed from the atomizer bottle at 45°C angles to the wound bottom from a distance of 1 cm.

We evaluated the condition of the wounds for signs of inflammation: edema, hyperemia, exudation, infiltration of surrounding tissues and covered the wounds with perforated plastic wrap after each procedure.

Morphological Analysis

On a post-operative day 4, the wound tissues were excised for histological examination. Biological samples were fixed in neutral buffered 10% formalin and embedded into paraffin blocks. 4–5 μm thick paraffin sections were stained with hematoxylin and eosin, picrosirius red, toluidine blue, and by Mallory. The obtained microscopic slides were examined with a universal LEICA DM4000 B LED microscope equipped with a LEICA DFC7000 T digital video camera (Leica Microsystems, Germany) by standard light and phase contrast microscopy methods. Sections stained with picrosirius red were examined by polarized light microscopy to determine the maturity and architectonics of collagen fibers. Anisotropy in the red spectrum suggested the predominance of type I collagen in the green spectrum - type III collagen.[33,34]

Histological slides of wound tissues were evaluated by the semi-quantitative analysis system described earlier. In each section, signs of inflammation (exudation, presence of bacterial colonies, inflammatory infiltration, microcirculation disorders) and regeneration (angiogenesis, fibroblast proliferation, volume, and maturity of granulation tissue) were assessed on a 5-point scale (0 - no, 4 - maximum intensity). Measurement of the thickness of the fibrin clot and granulation tissue layer was performed at 5 random points of each preparation using Leica Application Suite, version 4.9.0 (Build 129).

The number of mast cells in sections stained with toluidine blue was calculated in 10 fields of view at a magnification of 400x. We used the following formula to determine the functional activity of the mast cells: $X=((T0x0)+(T1x1)+(T2x2)+(T3x3))/n$, where X – functional activity index, To – cells with separately distinguishable granules and an incompletely disguised nucleus, T1 – mast cell with minor portions of granules scattered around the cell, T2 – cells with a distinct nucleus, well-distinguishable granules in and around the cell, T3 – cells with a distinct nucleus, well-distinguishable granules in and around the cell.[35]

Immunohistochemical Study

Paraffin-embedded tissues were sectioned into 4 μm slides for immunohistochemical (IHC) analysis. The routine procedure of deparaffinization, dehydration, and rehydration was performed followed by heat-induced epitope retrieval (pH = 6.0 sodium citrate solution, 30 min in 80°C water bath). Then, 3% H_2O_2 was added to deactivate the endogenous peroxidase and background Block (Cell Marque, Germany) for blocking nonspecific binding. Subsequently, the tissue sections were treated with primary antibodies against vimentin (MA5-11883, Invitrogen). Horseradish peroxidase-conjugated goat antibody was applied as the secondary (G-21040, Invitrogen). After that, the staining was visualized

with the DAB (34002, Thermo Scientific), counter-stained with hematoxylin. Slides were examined and photographed by two blinded pathologists. To assess vimentin content, only granulation tissue areas at the place of alteration were evaluated and shot at 400× magnification. Deep learning-based segmentation of vimentin-positive cells in the images was performed with ilastik (version 1.3.3) by manually labeling pixels as belonging to one of three classes: fibroblasts (brown elongated cells), other (cells and matrix stained with hematoxylin), and background (mostly white pixels). The vimentin expression was evaluated semi-quantitatively by a scoring system: 0 – negative expression; 1 – singular non-oriented cells; 2 – thin layer (less than 100 μm) of vimentin-positive cells with parallel orientation; 3 – thick layer (over 100 μm) of vimentin-positive cells with parallel orientation.

Statistical Analysis

Experimental data analysis was carried out with the standard software package GraphPad Prism version 8.00 for Windows (GraphPad Software, Inc.). Normal distribution of quantitative data (intensity of inflammation, the intensity of regeneration, thickness of the granulation tissue layer, vimentin expression, index of functional activity of mast cells) was checked using Shapiro–Wilk's test for normal distribution. Intergroup differences in the intensity of inflammation and regeneration, expression of vimentin, and the index of functional activity of mast cells were analyzed using the Kruskal–Wallis test with the post-hoc Dunn's test. Intergroup differences in granulation tissue layer thickness and ovality ratio were analyzed using a one-way ANOVA with Tukey's post-hoc test. The results for data distribution were illustrated as normal QQ plots (Supplementary Figure 1). The intensity of inflammation and regeneration, the thickness of the granulation tissue layer, the functional activity of mast cells were presented as boxes with whiskers with values of medians and 95% confidence intervals. The results of IHC study were presented as a scatter plot graph. The significant level of differences p was assessed at the value <0.05.

Results

Spray Characterization

The mean spray ovality ratio was 1.03± 0.05; it did not differ between DNIC solutions of various concentrations (Figure 1, left). So, all tested concentrations had good sprayability. DNIC dosage in the single sprayed volume was stable and equaled 0.1±0.043 μg. Using the Teflon ring with a fixed inner diameter 30mm and DNIC solutions stained with methylene blue, we determined that the optional distance for spraying the whole dose to the wound area is 1 cm at 45° spray angle.

The spectrophotometric evaluation revealed linear DNIC degradation in the solution, leaving only 30% of the initial concentration after 5 hours. However, DNIC concentration was stable for the first 30 minutes (Figure 1, central). Complete degradation of DNIC occurred after 6 hours (at pH = 7.0), resulted in nitrite accumulation (Figure 1, right). Because of low stability, freshly prepared solutions of standard concentrations were aliquoted and stored at −70°C until the application to prevent degradation.
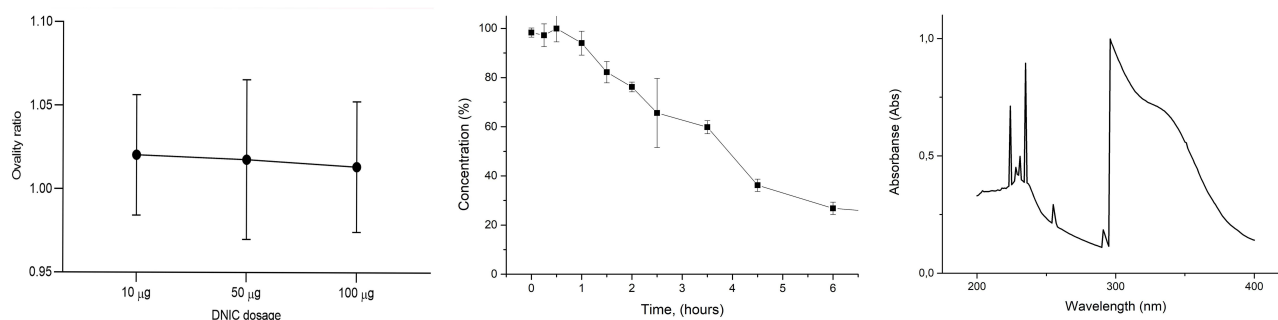

Figure 1 Ovality ratio of spray patterns of DNIC solutions (left). DNIC degradation in 37°C PBS (central), the means and standard deviation. Absorption spectrum of nitrites (right).

Gross Evaluation

All animals survived the period of the experiment. On the next day after the surgery, the general condition of the animals was satisfactory. We noticed slight edema without hyperemia in the wound areas. The wound bottoms were clean and pink with a smooth shining surface, covered with a small amount of transparent serous exudate (Supplementary Figure 2A, E, I and M).

On a post-operative day 2, the wound bottoms were hyperemic and covered with a moderate amount of fibrin along the edges in half of the animals in the control group (Supplementary Figure 2B). In the other half of the control rats and in the experimental group animals, the wounds had smooth, slightly hyperemic wound surfaces with an insignificant amount of fibrin along the edges. In some wounds, there was a slight volume of transparent and odorless exudate (Supplementary Figure 2F, J and N).

On a post-operative day 3, 5 out of 6 control wound bottoms were diffusely covered with a thick layer of fibrin and contained up to 0.03 mL of an opaque exudate (Supplementary Figure 2C). In only one case, the wound was characterized by a smooth, shiny surface with a small amount of serous exudate. In study group 2 (10 μg), serous exudate was detected in half of the wound bottoms, while the wound surfaces in other animals were hyperemic with insignificant loose fibrin along the edges (Supplementary Figure 2G). In study group 3 (50 μg), the wound bottoms were similar to the experimental wound on post-operative day 2 (Supplementary Figure 2K). Half of the animals of study group 4 (100 μg) had abundant depositions of loose fibrin, transparent and odorless exudate along the wound edges. The other 3 wound bottoms were moderately hyperemic and had a shiny surface (Supplementary Figure 2O).

On post-operative day 4, the control wound bottoms were similar to those on the third day after the operation (Supplementary Figure 2D). Most of the wounds in study group 2 (10 μg) were covered with a thin film of loose fibrin and a minor volume of odorless, opaque exudate (Supplementary Figure 2H). In study group 3 (50 μg), most of the wounds had clean, shiny bottoms covered with an insignificant amount of serous exudate (Supplementary Figure 2L). In study group 4 (100 μg), the fibrin film was observed in 4 out of 6 animals and completely covered the wound bottoms in 2 rats (Supplementary Figure 2P). The wounds in the other 2 animals had smooth and shiny bottoms.

Histological Analysis

In the control group, the wounds of almost all animals had bacterial contamination. The fibrin clot was thick and was stained pale blue by Mallory method (Figure 2A and B). The inflammatory changes were moderate and are mainly included leukocyte shaft, diffuse tissue infiltration with lymphocytes and macrophages, leukostasis, and productive vasculitis. The wound bottoms had areas of hemorrhage and signs of stasis and sludge in singular blood vessels. The granulation tissue had extremely low maturity. In 3 out of 6 cases, it was present only as separate islets, while fibrin significantly predominated over collagen fibers, which was confirmed by Mallory staining and phase-contrast microscopy (Figure 2B and 3A, B). Under polarized light, anisotropy was practically absent because of the immaturity of collagen. Only singular thin fibers gave green shining (collagen type III) (Figure 2C and Figure 3C).

In study group 2 (10 μg), bacterial contamination was observed in 4 out of 6 rats. The fibrin clot contained a loose fibrin network with signs of fibrosis. Diffuse leukocyte infiltration, leukostasis, and productive vasculitis indicated an intensive inflammatory process in this group (Figure 2D). The thickness of the granulation tissue layer was 108% higher than in the control, while the regeneration signs were also significantly higher. Vertically oriented capillaries were identified in one animal indicating accelerated maturation of the wound tissue (Figure 3D).

When stained by Mallory, the cells predominated over a fibrous component of the granulation tissue (Figures 2E and 3E). Phase-contrast microscopy revealed that the superficial layer of the wound tissue majorly consisted of fibrin. However, the underlying granulation tissue had a distinct layer of thin, newly formed collagen fibers (Figure 3F). The same was confirmed by polarized light microscopy. The fibers gave not only green but also red anisotropy, indicating the superior maturity of the granulation tissue to the control (Figure 2F).

In study group 3 (50 μg), the fibrin clot was significantly thinner than in the previous groups and comprised a loose network of fibrin. Singular microbial colonies were determined in 3 out of 6 cases. Leukocyte infiltration was moderate,
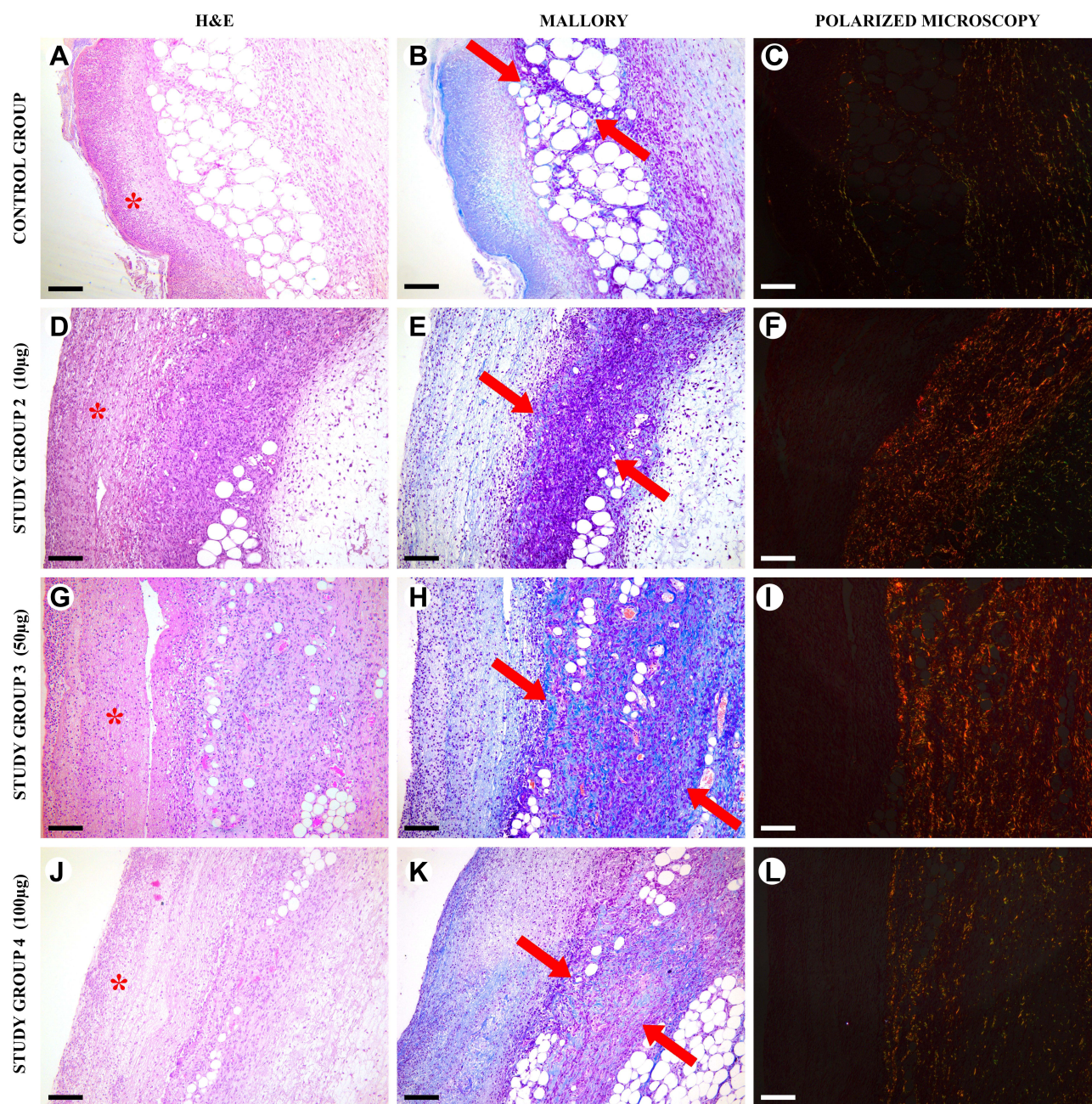
	H&E	MALLORY	POLARIZED MICROSCOPY

Figure 2 Histology of the wounds at post-operative day 4, simple light and polarized light microscopy, hematoxylin and eosin (**A, D, G** and **J**), Mallory method (**B, E, H** and **K**) and picrosirius red (**C, F, I** and **L**) staining, scale bar – 100 μm. (**A**) – focuses of immature granulation tissue under the fibrin clot (*), (**B**) – focuses of immature granulation tissue (arrows) in the adipose tissue, (**C**) – low anisotropy of collagen fibers, (**D**) – a thick and dense fibrin clot (*), (**E**) – a layer of granulation tissue (arrows) with high content of cells, (**F**) – anisotropy of fibers of yellow and red color (**G**) – a fibrin clot (*), beneath – the layer of granulation tissue with full-blooded capillaries, (**H**) – a thick layer of granulation tissue (arrows) with dense content of fibers, (**I**) – predominance of red anisotropy, (**J**) – loose fibrin fibers infiltrated with neutrophils (*), (**K**) – a layer of granulation tissue (arrows) penetrates the adipose tissue, (**L**) – low red and yellow anisotropy of collagen fibers.

signs of microvascular disorders decreased. Immune cells were not observed in the blood vessels. All these findings showed a significantly lower intensity of inflammation than in the control ($p < 0.05$) (Figure 4).

The thickness of the granulation tissue layer was 140% higher than in the control. The granulation tissue was represented by vertically oriented blood vessels, longitudinally packed spindle-shaped fibroblasts, and newly formed collagen fibers, which were stained dark blue by Mallory method (Figures 2G and H, 3G and H). Phase-contrast microscopy revealed that thin, newly formed collagen fibers gradually replaced the fibrin network in the superficial layers of granulation tissue. The fibers prevailed in the deeper wound areas, oriented in parallel to each other, and were
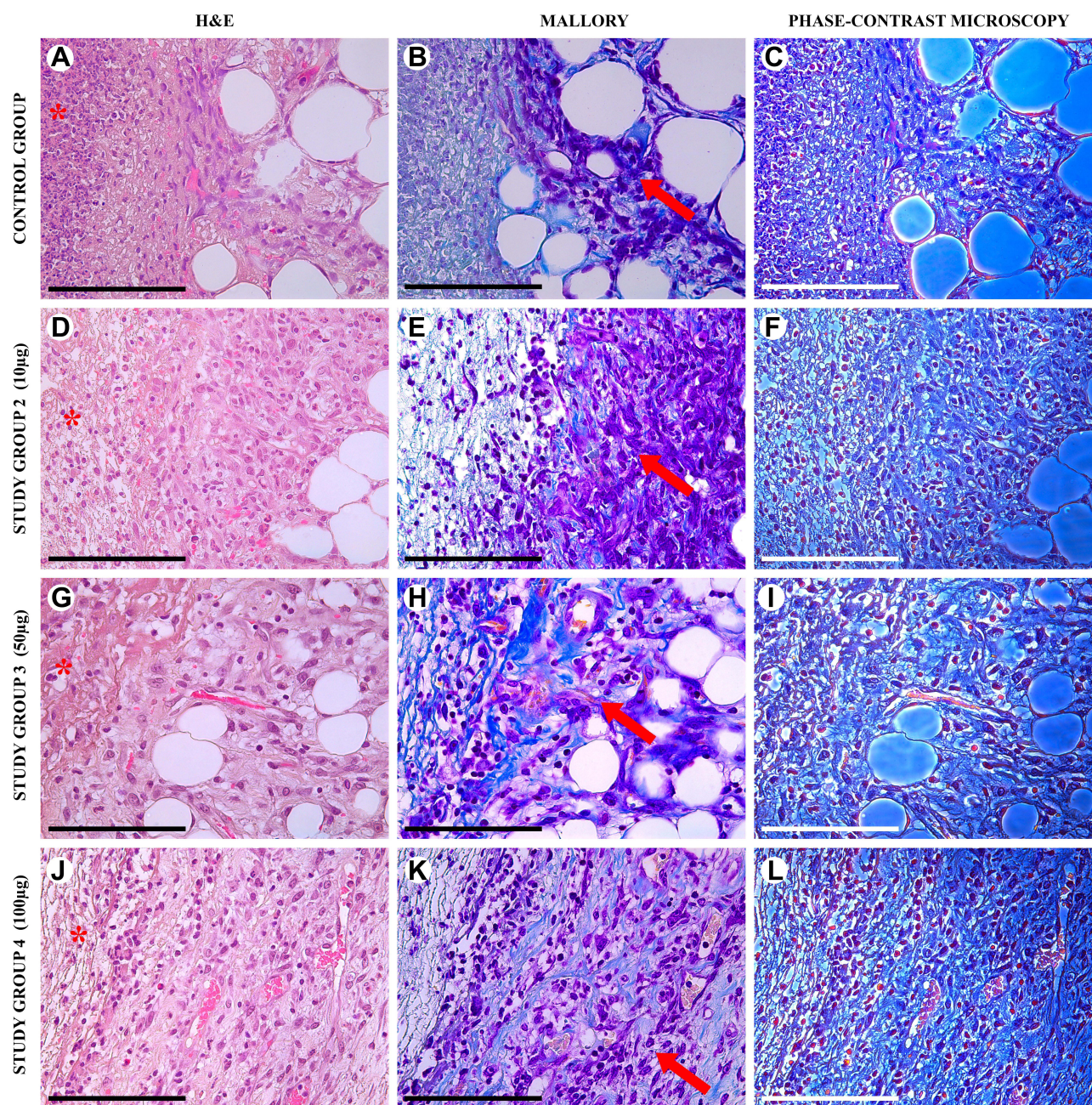
	H&E	MALLORY	PHASE-CONTRAST MICROSCOPY
CONTROL GROUP	A	B	C
STUDY GROUP 2 (10µg)	D	E	F
STUDY GROUP 3 (50µg)	G	H	I
STUDY GROUP 4 (100µg)	J	K	L

Figure 3 Histology of the wounds at post-operative day 4, simple light, phase-contrast, hematoxylin and eosin (**A, C, D, F, G, I, J** and **L**) and Mallory method (**B, E, H** and **K**) staining, scale bar – 100 μm. (**A**) – focuses of proliferating fibroblasts under the fibrin clot (*), (**B**) – proliferating fibroblasts (arrow) in the immature granulation tissue, (**C**) – bundles of collagen fibers among the fibrin network, (**D**) – fibrin clot (*), chaotically arranged fibroblasts and lymphocyte and macrophage infiltration in the granulation tissue, (**E**) – predominance of cells (arrow) over collagen fibers, (**F**) – a network of thin fibers, predominance of fibrin, (**G**) – granulation tissue with vertically oriented blood vessels under the fibrin network (*), (**H**) – high cellularity and collagen synthesis in the granulation tissue (arrow), (**I**) – interwoven thin collagen fibers, (**J**) – loose fibrin fibers, beneath – granulation tissue consisting of parallelly oriented fibroblasts and full-blooded vessels, (**K**) – predominance of collagen fibers (arrow) over cells, (**L**) – longitudinally oriented collagen fibers.

highly mature, which was confirmed by anisotropy in polarized light (Figures 2H and I, 3I). These findings suggest the mature state of the granulation tissue and its initial fibrous transformation.

In study group 4 (100 μg), the fibrin clot was relatively thick and contained a leukocyte shaft and a minor number of bacterial colonies. The granulation tissue layer was 112% thicker than in the control group. A moderate degree of maturity and growth through the subcutaneous fat characterized it (Figure 2J). It consisted of longitudinally oriented spindle-shaped fibroblasts, numerous newly formed full-bloodied capillaries, and collagen fibers (Figure 3J). When
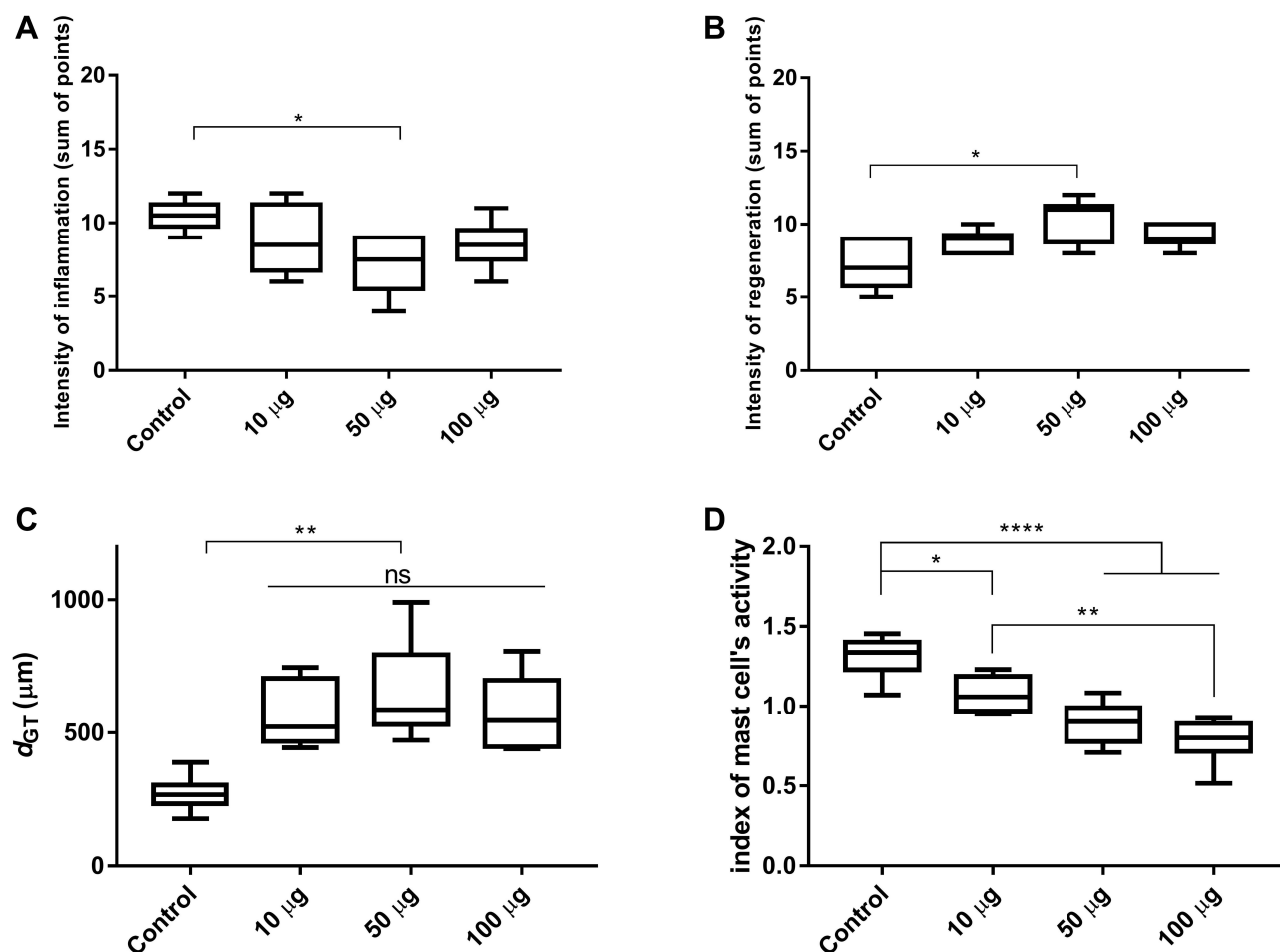
Figure 4 Morphometry of the wound tissues, Kruskal–Wallis (**A–D**) and one-way ANOVA (**C**) tests, boxes with whiskers, 95% CI. * – p < 0.05; **p < 0.01; ****p < 0.0001, n.s. – non-significant.

stained by Mallory, there were significantly fewer bright blue collagen fibers than fibrin, which was also visualized by phase-contrast microscopy (Figures 2K, 3K). Polarization microscopy revealed numerous but predominantly immature collagen fibers with green and yellow shining (Figure 2L and 3L).

We determined moderate vimentin expression in the sparsely distributed fibroblasts in the focuses of immature granulation tissue in the control (Figure 5). In the study group 2 (10 μg), the thin layer of granulation tissue consisted of numerous cells with high intensity of vimentin staining. In the study group 3 (50 μg), the spindle-shaped, parallelly oriented, strongly positive for vimentin fibroblasts predominated in the thick granulation tissue layer compared to the control (p < 0.05). In study group 4 (100 μg), the vimentin expression was similar to the control, but the granulation tissue layer was more mature and thick (Figure 6).

Distribution and Functional State of Mast Cells

In the control group, mast cells had a high secretory activity and were located both in the granulation tissue and in the subcutaneous fat (Figure 7A). The number of mast cells in the study group 2 (10 μg) was higher than in the control; however, the cells had a moderate degree of degranulation, while separately scattered granules were practically absent (Figure 7B). The index of functional activity in this group was significantly lower than in the control (p < 0.05). In study group 3 (50 μg), numerous mast cells localized mainly in subcutaneous fat. Their nuclei were not visualized because of the high density of granules. The functional activity index was significantly lower than in the control (p < 0.05) (Figure 7C). In study group 4 (100 μg), the number of mast cells in the subcutaneous fat was significantly higher than
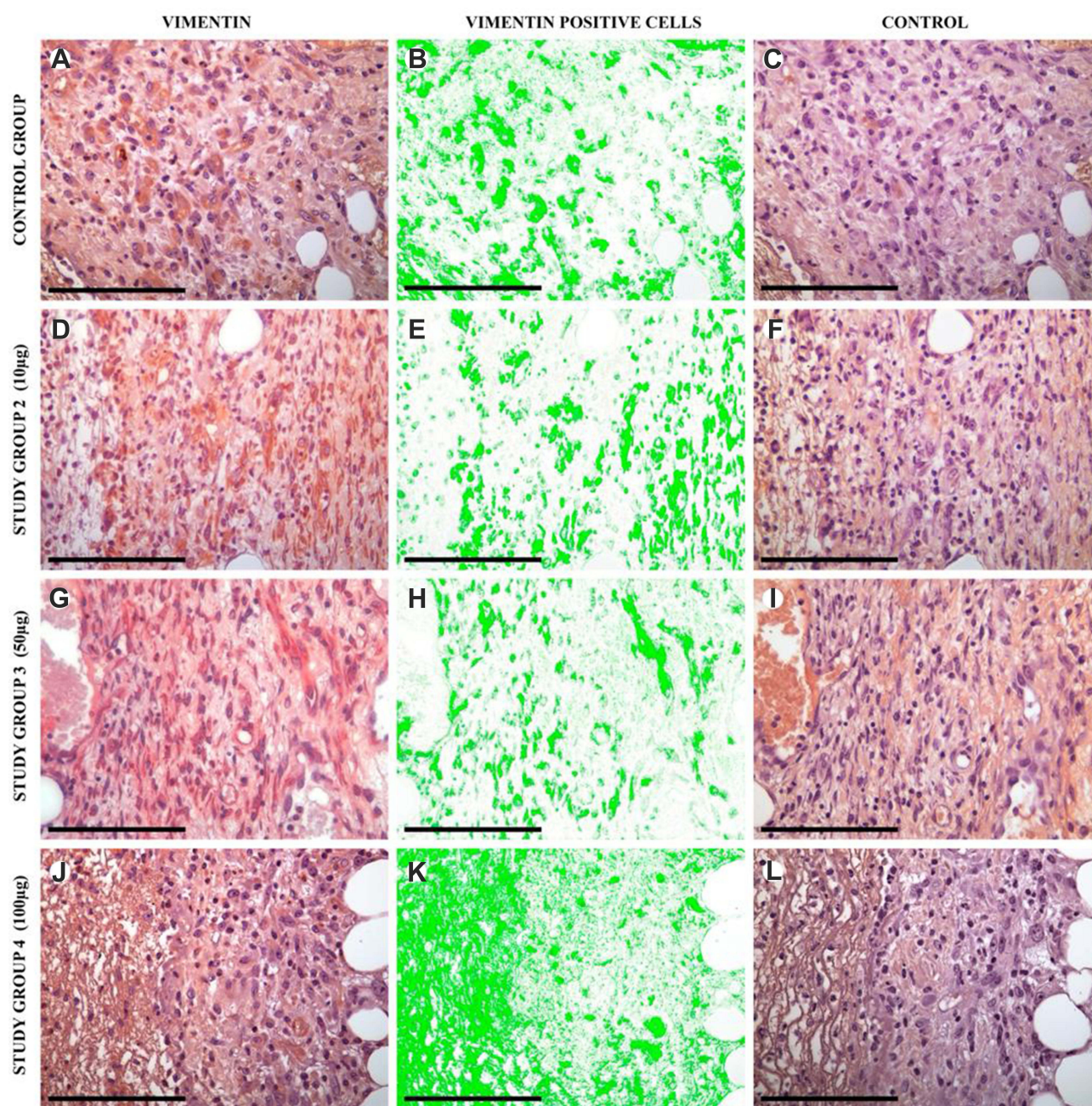
VIMENTIN	VIMENTIN POSITIVE CELLS	CONTROL

Figure 5 Vimentin expression in wound bottom tissues at post-operative day 4, scale bar – 100 µm. (**A–C**) – singular round vimentin-positive fibroblasts in granulation tissue, (**D–F**) – parallelly oriented elongated thin vimentin-positive fibroblasts in deep layer of granulation tissue, (**G–I**) – parallelly oriented thick bundles of vimentin-positive fibroblasts in granulation tissue, (**J–L**) – singular round vimentin-positive fibroblasts under falsely positively stained fibrin clot.

in the granulation tissue. However, the cells had a low or moderate functional activity, determining a low functional activity index compared to the control ($p < 0.01$) and the study group 2 ($p < 0.05$) (Figure 7D).

Discussion

According to previously published studies, DNIC has beneficial effects on wound healing.[7,13,15,16,28,36,37] Nevertheless, intravenous drug administration for wound treatment is not justified due to the under-investigated side effects and pharmacokinetics.[13] At the same time, the local delivery through direct injections of the wound bottoms promotes excessive trauma and hydration of wound tissues.[28,36] The spray form has the potential to become an effective way to
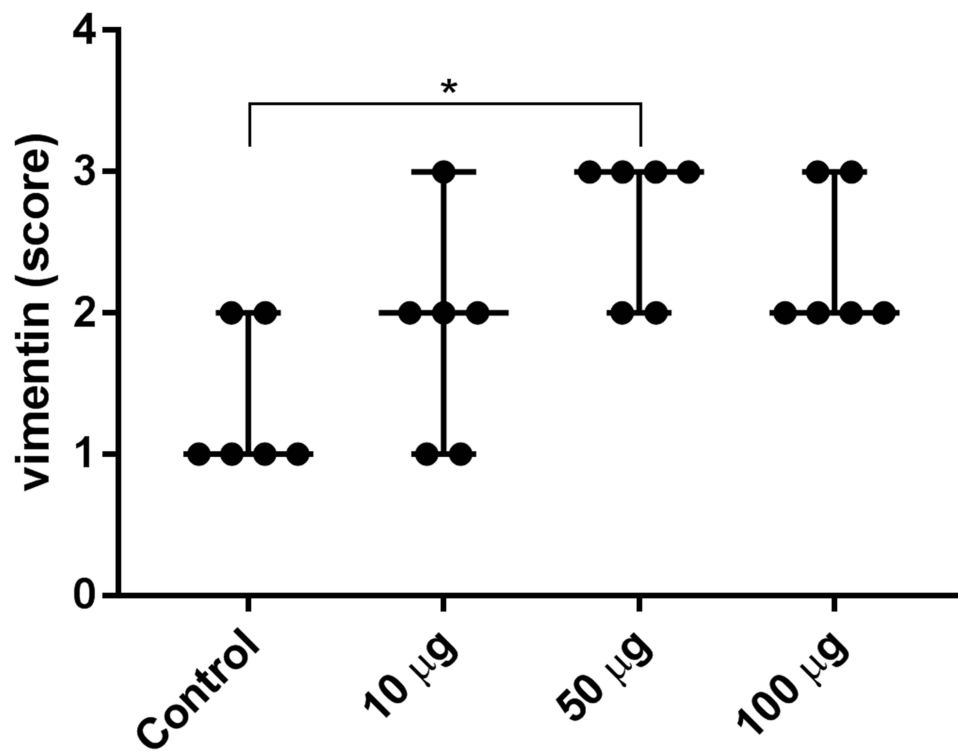
Figure 6 Semi-quantitative morphometry of vimentin expression in granulation tissue at post-operative day 4, Kruskal–Wallis test, boxes with whiskers, 95% CI. * – p < 0.05.
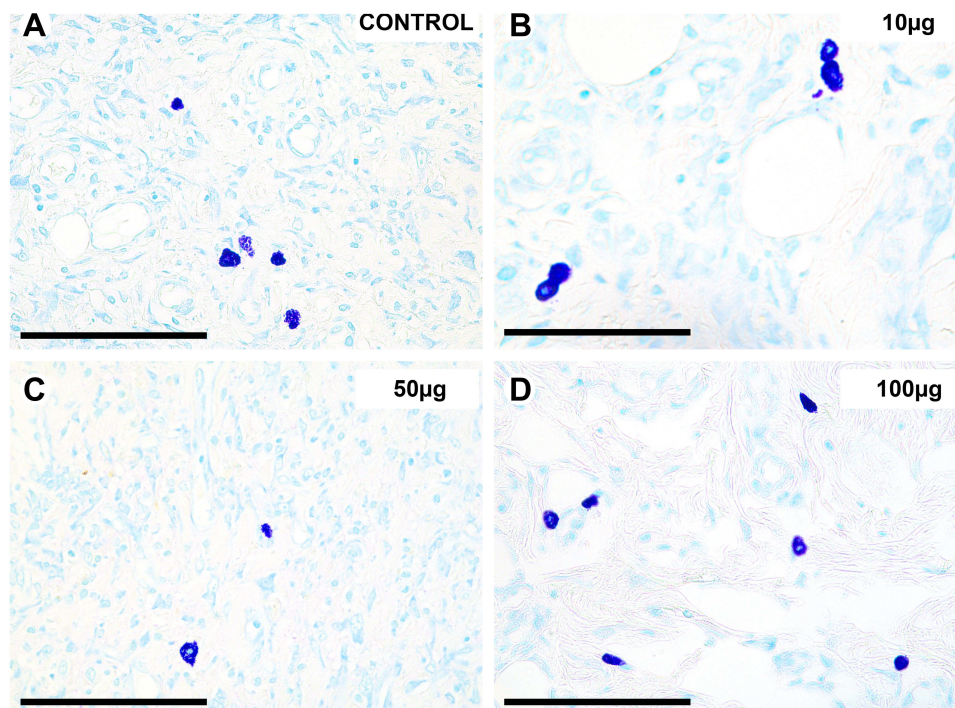

Figure 7 Distribution and functional state of mast cells in wound bottoms at post-operative day 4, toluidine blue staining, scale bar – 100 μm. (**A**) – mast cells with signs of degranulation in the granulation tissue, (**B**) – mast cells with well-identifiable nucleus and single granules, (**C**) – singular mast cells located near parallelly oriented fibroblasts and collagen fibers, (**D**) – mast cells with dense granules.

apply DNIC for wound treatment in clinical practice, as it provides uniform distribution of the active substance and does not require expensive equipment for its synthesizing.

The development of a simple, accessible and easy-to-use form of DNIC delivery has been a scientific challenge for many years. Shekhter et al synthesized a collagen-based scaffold containing 4 μM DNIC with a glutathione ligand, which facilitated wound regeneration and complete epithelialization 4 days earlier than in spontaneously healing wounds.[37] The inflammatory changes were less pronounced and the granulation tissue matured faster in the experimental group than in the control. However, the rapid release of DNIC from the implant limited its pro-regenerative effects.

In the present study, a spray form of delivery of DNIC with a glutathione ligand facilitated wound healing on macro-, and microscopic levels. DNIC at the dose of 10 μg stimulated cellular proliferation and granulation tissue growth but was not sufficient for the anti-inflammatory effect or acceleration of the collagen synthesis. Spray with 50 μg of DNIC had the most beneficial effects on reduction of the inflammation and promotion of the growth and maturation of granulation tissue. At the same time, 100 μg dose of DNIC was excessive, since it did not have a comparable effect on the thickness and maturity of granulation tissue while increasing the inflammation in comparison with the DNIC dose of 50 μg. The pathological intensification of oxidative processes can explain this effect, the inhibition of cellular migration, fibroblast proliferation, and angiogenesis in the wound tissues.

In the early stages of wound healing, NO interacts with superoxide forming peroxynitrite causing a decrease of the wound tissue pH. It reveals as inflammatory reaction facilitating and greater bactericidal effect.[6,38–41] Also, NO stimulates the production of chemokines for neutrophils by macrophages and monocytes by regulating NF-kB gene expression.[38] As the concentration of NO increases, the modulation of NF-kB stops, the production of pro-inflammatory cytokines decreases and the antioxidant defense system activates.[38]

Low concentrations of NO bind to the heme center of the guanylate cyclase enzyme (sGC) in the vessels and trigger the cGMP-dependent cascade. It activates ERK1/2 and stimulates endothelial cell proliferation and angiogenesis.[11,13] Moreover, NO signaling affects the synthetic activity of fibroblasts, defining the speed and period of wound healing.[16,42]

In this study, we analyzed the functional activity of mast cells and revealed the inverse relationship between the dose of DNIC and the index of degranulation. Mast cells enhance local recruitment of neutrophils, which can accelerate the inflammatory phase of wound healing or lead to excessive tissue damage.[43] DNIC application at the doses of 50 μg and 100 μg possibly prevented this complication.

At the same time, mast cell stimulation with IgG1 immune complexes indirectly accelerates the transition of the inflammatory phase to the regenerative phase of wound healing. TNF secreted by mast cells regulates the expression of IL-4 and IL-13, which induce repolarization of macrophages from pro-inflammatory M1 to pro-regenerative M2 type. In addition, mast cells secrete lidocaine-2, a deficiency of which can lead to impaired wound healing.[44] This can explain the absence of a direct correlation between the intensity of regeneration and the minimum functional activity of mast cells in the study group 4 (100 μg).

In this article, we investigated the basic mechanisms through which the DNIC spray could accelerate wound healing. The need for ready-made solutions storage frozen and thaw them before use associates with the limitations of our research. So, the DNIC formula requires modifications to increase the period of this molecule's stability. After that, we intend to continue the research project on more specific models, in particular, on models of chronic non-healing wounds and large-area burns. We focus on the development of pro-regenerative off-the-shelf sprays for patient care. We hope that such a delivery form will make it possible to effectively apply the DNIC solution regardless of the area of damage and increase the frequency of treatment of the wound surface up to several times a day.

Conclusion

The present histological and morphometric study proved that DNIC spray at a dose of 50 μg accelerates wound healing. The local Nitric Oxide delivery to wound tissues was highly effective and easy to use.

Abbreviations

NO, nitric oxide; DNIC, dinitrosyl iron complex; ONOO-, peroxynitrite radical; H&E, hematoxylin and eosin staining.

Ethical Approval and Consent to Participate

Acknowledgments

Disclosure

The authors report no conflicts of interest in this work.

References

1. Daiber A, Xia N, Steven S, et al. New therapeutic implications of endothelial nitric oxide synthase (eNOS) function/dysfunction in cardiovascular disease. *Int J Mol Sci*. 2019;20(1):187. doi:10.3390/ijms20010187
2. Gantner BN, LaFond KM, Bonini MG. Nitric oxide in cellular adaptation and disease. *Redox Biol*. 2020;34:101550. doi:10.1016/j. redox.2020.101550
3. Dawson TM, Dawson VL. Nitric oxide signaling in neurodegeneration and cell death. In: *Advances in Pharmacology*. Vol. 82. Elsevier; 2018:57–83.
4. Hossain S, Nisbett L-M, Boon EM. Discovery of two bacterial nitric oxide-responsive proteins and their roles in bacterial biofilm regulation. *Acc Chem Res*. 2017;50(7):1633–1639. doi:10.1021/acs.accounts.7b00095
5. Yang T, Zelikin AN, Chandrawati R. Progress and promise of nitric oxide-releasing platforms. *Adv Sci*. 2018;5(6):1701043. doi:10.1002/advs.201701043
6. Bogdan C. Regulation of lymphocytes by nitric oxide. In: *Suppression and Regulation of Immune Responses*. Springer; 2010:375–393.
7. Shekhter AB, Serezhenkov VA, Rudenko TG, Pekshev AV, Vanin AF. Beneficial effect of gaseous nitric oxide on the healing of skin wounds. *Nitric Oxide*. 2005;12(4):210–219. doi:10.1016/j.niox.2005.03.004
8. Iwata M, Inoue T, Asai Y, et al. The protective role of localized nitric oxide production during inflammation may be mediated by the heme oxygenase-1/carbon monoxide pathway. *Biochem Biophys Rep*. 2020;23:100790. doi:10.1016/j.bbrep.2020.100790
9. Shekhter AB, Pekshev AV, Vagapov AB, et al. Dose-dependent effect of plasma-chemical NO-containing gas flow on wound healing. An experimental study. *Clin Plasma Med*. 2020;19–20:100101. doi:10.1016/j.cpme.2020.100101
10. Lee J, Hlaing SP, Cao J, et al. In situ hydrogel-forming/nitric oxide-releasing wound dressing for enhanced antibacterial activity and healing in mice with infected wounds. *Pharmaceutics*. 2019;11(10):496. doi:10.3390/pharmaceutics11100496
11. Duchesne C, Banzet S, Lataillade JJ, Rousseau A, Frescaline N. Cold atmospheric plasma modulates endothelial nitric oxide synthase signalling and enhances burn wound neovascularisation. *J Pathol*. 2019;249(3):368–380. doi:10.1002/path.5323
12. Yang L, Feura ES, Ahonen MJR, Schoenfisch MH. Nitric oxide–releasing macromolecular scaffolds for antibacterial applications. *Adv Healthcare Mater*. 2018;7(13):1800155. doi:10.1002/adhm.201800155
13. Chen Y-J, Wu S-C, Wang H-C, et al. Activation of angiogenesis and wound healing in diabetic mice using NO-delivery dinitrosyl iron complexes. *Mol Pharm*. 2019;16(10):4241–4251. doi:10.1021/acs.molpharmaceut.9b00586
14. Seabra AB, Justo GZ, Haddad PS. State of the art, challenges and perspectives in the design of nitric oxide-releasing polymeric nanomaterials for biomedical applications. *Biotechnol Adv*. 2015;33(6):1370–1379. doi:10.1016/j.biotechadv.2015.01.005
15. Vanin AF. Dinitrosyl iron complexes with thiol-containing ligands as a "working form" of endogenous nitric oxide. *Nitric Oxide*. 2016;54:15–29. doi:10.1016/j.niox.2016.01.006
16. Vanin AF. *Dinitrosyl Iron Complexes as a "Working Form" of Nitric Oxide in Living Organisms*. Cambridge Scholars Publishing; 2019.
17. Vanin AF, Poltorakov AP, Mikoyan VD, Kubrina LN, Burbaev DS. Polynuclear water-soluble dinitrosyl iron complexes with cysteine or glutathione ligands: electron paramagnetic resonance and optical studies. *Nitric Oxide*. 2010;23(2):136–149. doi:10.1016/j.niox.2010.05.285
18. Mikoyan VD, Burgova EN, Borodulin RR, Vanin AF. The binuclear form of dinitrosyl iron complexes with thiol-containing ligands in animal tissues. *Nitric Oxide*. 2017;62:1–10. doi:10.1016/j.niox.2016.10.007
19. Timoshin AA, Lakomkin VL, Abramov AA, et al. The hypotensive effect of the nitric monoxide donor Oxacom at different routs of its administration to experimental animals. *Eur J Pharmacol*. 2015;765:525–532. doi:10.1016/j.ejphar.2015.09.011
20. Liu T, Zhang M, Terry MH, et al. Hemodynamic effects of glutathione-liganded binuclear dinitrosyl iron complex: evidence for nitroxyl generation and modulation by plasma albumin. *Mol Pharmacol*. 2018;93(5):427–437. doi:10.1124/mol.117.110957
21. Pisarenko O, Studneva I, Timoshin A, Veselova O. Protective efficacy of dinitrosyl iron complexes with reduced glutathione in cardioplegia and reperfusion. *Pflugers Arch*. 2019;471(4):583–593. doi:10.1007/s00424-018-02251-2
22. Kapelko VI, Lakomkin VL, Abramov AA, et al. Protective effects of dinitrosyl iron complexes under oxidative stress in the heart. *Oxid Med Cell Longev*. 2017;2017:1–10. doi:10.1155/2017/9456163
23. Andreyev-Andriyevsky AA, Mikoyan VD, Serezhenkov VA, Vanin AF. Penile erectile activity of dinitrosyl iron complexes with thiol-containing ligands. *Nitric Oxide*. 2011;24(4):217–223. doi:10.1016/j.niox.2011.04.008
24. Burgova EN, Tkachev NA, Adamyan LV, et al. Dinitrosyl iron complexes with glutathione suppress experimental endometriosis in rats. *Eur J Pharmacol*. 2014;727:140–147. doi:10.1016/j.ejphar.2014.01.002
25. Burgova EN, Khristidis YI, Kurkov AV, et al. The inhibiting effect of dinitrosyl iron complexes with thiol-containing ligands on the growth of endometrioid tumours in rats with experimental endometriosis. *Cell Biochem Biophys*. 2019;77(1):69–77. doi:10.1007/s12013-019-00865-6
26. Wu S-C, Lu C-Y, Chen Y-L, et al. Water-soluble dinitrosyl iron complex (DNIC): a nitric oxide vehicle triggering cancer cell death via apoptosis. *Inorg Chem*. 2016;55(18):9383–9392. doi:10.1021/acs.inorgchem.6b01562

27. Giliano NY, Konevega LV, Noskin LA, Serezhenkov VA, Poltorakov AP, Vanin AF. Dinitrosyl iron complexes with thiol-containing ligands and apoptosis: studies with HeLa cell cultures. *Nitric Oxide*. 2011;24(3):151–159. doi:10.1016/j.niox.2011.02.005

28. Solovieva AB, Vanin AF, Shekhter AB, et al. Is it possible to combine photodynamic therapy and application of dinitrosyl iron complexes in the wound treatment? *Nitric Oxide*. 2019;83:24–32. doi:10.1016/j.niox.2018.12.004

29. Ibrahim SA. Spray-on transdermal drug delivery systems. *Expert Opin Drug Deliv*. 2015;12(2):195–205. doi:10.1517/17425247.2015.961419

30. Sritharadol R, Nakpheng T, Wan Sia Heng P, Srichana T. Development of a topical mupirocin spray for antibacterial and wound-healing applications. *Drug Dev Ind Pharm*. 2017;43(10):1715–1728. doi:10.1080/03639045.2017.1339077

31. Bateman SD. Topical haemoglobin spray for diabetic foot ulceration. *Br J Nurs*. 2015;24(Sup12):S24–S29. doi:10.12968/bjon.2015.24.Sup12.S24

32. Peirce SC, Carolan-Rees G. ReCell® spray-on skin system for treating skin Loss, scarring and depigmentation after burn injury: a NICE medical technology guidance. *Appl Health Econ Health Policy*. 2019;17(2):131–141. doi:10.1007/s40258-018-00457-0

33. Alves A, Attik N, Bayon Y, et al. Devising tissue ingrowth metrics: a contribution to the computational characterization of engineered soft tissue healing. *Biomed Mater*. 2018;13(3):035010. doi:10.1088/1748-605X/aaa9d4

34. Coelho PGB, Souza M, Conceição LG, Viloria MIV, Bedoya SAO. Evaluation of dermal collagen stained with picrosirius red and examined under polarized light microscopy. *An Bras Dermatol*. 2018;93(3):415–418. doi:10.1590/abd1806-4841.20187544

35. Lindner DP, Poberiy IA, Rozkin MY, Efimov VS. Morphometrical analysis of mast cell populations. *Arkh Patol*. 1980;42:60–64.

36. Shekhter A, Rudenko T, Serezhenkov V, Vanin A. Dinitrosyl-iron complexes with cysteine or glutathione accelerate skin wound healing in animals. *Biofizika*. 2007;52(3):539–547.

37. Shekhter AB, Rudenko TG, Istranov LP, Guller AE, Borodulin RR, Vanin AF. Dinitrosyl iron complexes with glutathione incorporated into a collagen matrix as a base for the design of drugs accelerating skin wound healing. *Eur J Pharmaceut Sci*. 2015;78:8–18. doi:10.1016/j.ejps.2015.06.002

38. Kobayashi Y. The regulatory role of nitric oxide in proinflammatory cytokine expression during the induction and resolution of inflammation. *J Leukoc Biol*. 2010;88(6):1157–1162. doi:10.1189/jlb.0310149

39. Thomas DD, Heinecke JL, Ridnour LA, et al. Signaling and stress: the redox landscape in NOS2 biology. *Free Radic Biol Med*. 2015;87:204–225. doi:10.1016/j.freeradbiomed.2015.06.002

40. Ghimire K, Altmann HM, Straub AC, Isenberg JS. Nitric oxide: what's new to NO? *Am J Physiol Cell Physiol*. 2017;312(3):C254–C262. doi:10.1152/ajpcell.00315.2016

41. Ridnour LA, Windhausen AN, Isenberg JS, et al. Nitric oxide regulates matrix metalloproteinase-9 activity by guanylyl-cyclase-dependent and-independent pathways. *Proc Natl Acad Sci*. 2007;104(43):16898–16903. doi:10.1073/pnas.0702761104

42. Schäffer M, Efron PA, Thornton FJ, Klingel K, Gross SS, Barbul A. Nitric oxide, an autocrine regulator of wound fibroblast synthetic function. *J ImmunoL*. 1997;158(5):2375–2381.

43. Galli SJ, Borregaard N, Wynn TA. Phenotypic and functional plasticity of cells of innate immunity: macrophages, mast cells and neutrophils. *Nat Immunol*. 2011;12(11):1035. doi:10.1038/ni.2109

44. Chompunud Na Ayudhya C, Roy S, Thapaliya M, Ali H. Roles of a mast cell–Specific receptor MRGPRX2 in host defense and inflammation. *J Dent Res*. 2020:0022034520919107. doi:10.1177/0022034520919107